# Fast Trajectory Tracking of a Flexure-based, Multi-Axis Nanopositioner with 50 mm Travel

Nilabh K Roy[1*] and Michael A Cullinan[2]

[1]*Corresponding author- Mechanical engineering department, University of Texas at Austin; nilabh.roy@utexas.edu

[2] Mechanical engineering, University of Texas at Austin; michael.cullinan@austin.utexas.edu; 204 E. Dean Keeton Street, Stop C2200 ETC 4.154, Austin, Texas 78712-1591

*Abstract*-The precise, high-speed control of nanopositioning stages is critical for many microscale additive manufacturing systems, such as microscale selective laser sintering (µ-SLS), where high throughput is needed. In µ-SLS, the positioning stage requires achieving 10 Hz steps with sub-100 nm accuracy and a travel range of 50 mm. The open loop resolution and settling time of the flexure stage presented in the study are found to be 63 nm and 1.27s respectively. This settling time is too large for its application in high throughput µ-SLS. To improve the tracking performance of the stage for fast varying signals upto 10 Hz and achieve better resolution, this paper presents the design of a finite horizon linear quadratic regulator controller for the XY stage. Owing to the good damping properties of the controller, the resolution is improved to 8 nm and input signals with 10 Hz frequency are effectively tracked. With the addition of a resonant shifting control, the tracking bandwidth is improved to 23 Hz. The paper presents a unique combination of low cost, large travel, sub 10 nm resolution and high bandwidth XY positioning system, which is not to be found in either off-the-shelf nanopositioning stages or in research labs.

Keywords: Long travel, Flexure stage, Linear Quadratic Control, Microscale Selective Laser sintering, Nanopositioning, Resonance damping, Tracking

## I. INTRODUCTION

Microscale additive manufacturing (AM) using metals and ceramics can have a multitude of applications in the aerospace, electronics, and medical device industries. Unfortunately, current commercially available metal AM tools either have feature-size resolutions of >100 µm, which is too large to precisely control the microstructure of the parts they produce or can only produce two dimensional structures. To overcome this problem, a novel micro-AM technique called microscale selective laser sintering (µ-SLS) has been developed [1], [2]. This process allows development of 3D parts with 1 µm sized features while still maintaining the part complexity and throughput of the traditional selective laser sintering (SLS) process. µ-SLS works in much the same way as traditional SLS process except that nanoscale powders in a dispersion are used instead of micro-particles in the powder bed. Fast lasers and scanning micro-mirror arrays are also used to achieve microscale feature resolutions. The system consists of six critical components (see supplementary Fig. S1) : (1) the spreader mechanism to generate the powder bed, (2) the optical system to write features into the powder bed, (3) the laser system to sinter the particles, (4) the stepper system to move the powder bed under the optical system, (5) a vacuum chuck to hold the build plate in place and ensure that it does not deform during the coating or sintering process, and (6) a vibration isolation system to reduce outside influences that could damage the part quality.

To achieve the desired accuracy and throughput, it is required to move the powder bed under the optical system as fast as possible to minimize the latency and maximize the up-time for actual sintering. Thus, an XY nanopositioner forms an integral part of the µ-SLS system. The XY nanopositioning stage is required to align the sample wafer under the optical system and to scan the sample under the micro-mirror based optical system with sub-micron accuracy and repeatability [3]. The micro-mirror based optical sub-system can only pattern an area of 2 mm by 1 mm at once. To pattern a two-inch wafer under the optical sub-system, XY stage needs to have a range of 50 mm along both X and Y directions. The stage is expected to move in a maximum step size of 2 mm with accuracy close to the desired feature resolution of 1µm. Although existing off-the-shelf nanopositioning systems can achieve smaller than 5 nm motion quality (see Table 1), they are limited in their range to a few hundred microns per axis [4], [5]. On the other hand, traditional motion systems (usually based on rolling element bearings) can provide a large range (~1 to 100 mm), but are limited to a motion quality of >100 nm due to friction and backlash in system components [6], [7]. Other motion systems such as air bearing and magnetic bearing stages which can achieve the desired resolution and range, are significantly more expensive than the flexure-based stages. Table 1 lists the range and resolution (typically collected at input stepping frequency < 1 Hz) of some of the commercial and lab-developed XY nanopositioning stages.

Table 1. Range and resolution of various stages available commercially and developed in research labs

| Product | Range (mm x mm) | Resolution (nm) |
|---|---|---|
| PhysikInstrumente, P-546 [4] | 0.2 X 0.2 | 1 |
| U-723 PILine® Miniature XY Stage [6] | 22 X 22 | 100 |
| Mad City Labs, Nano-View [7] | 25 X 25 | 1000 |
| Hiemstra, David B., et al [8] | 10 X 10 | 20 |
| Awtar & Parmar[9] | 10 X 10 | 4 |
| Xu, Qingsong [10] | 11.7 X 11.7 | 200 |
| NPXY300-291 [5] | 0.3 X 0.3 | 1 |
| Shang, Jiangkun, et al [11] | 1.8 X 1.8 | 200 |

To realize a precision positioning with high accuracy, flexure-based compliant guiding mechanisms have been widely

employed due to the lack of friction and backlash in these systems [12], [13]. However, achieving a range >10 mm with sub-micron resolution and large bandwidth has proved to be challenging in the design of nanopositioning stages. In previous works, double parallelogram flexure (DPF) based designs have been developed that can achieve a motion range up to 12 mm [8]–[10], [14]. Awtar and Parmar[9] first presented the design of a long travel flexure based XY stage with a travel range of 10 mm and a closed loop resolution of 4 nm. Qingsong Xu[10] demonstrated a more compact design of a flexure XY stage with similar travel range of 11.7 mm X 11.7 mm, a closed loop resolution of 200 nm and a control bandwidth (30° lag) of 5.9 Hz. However, after an extensive literature review by the authors, no stage design could be found with a motion range as high as 50 mm and a sub 100 nm resolution barring the commercially available air bearing and magnetic bearing-based stages which are found to be an order of magnitude more expensive than flexure-based stages. Recently, a DPF bearing design for the XY stage was presented by the authors in [3], [15] with a 50 mm motion range along each axis but with a resonant frequency of only about 4 Hz. This tradeoff between range and bandwidth is because increasing the range of the flexure stage leads to an increase in inertia of the stage, consequently decreasing the resonance frequency and thus, limiting the operating speed of the nanopositioning stage.

Another difficulty with nanopositioning systems is the mechanical resonances arising from the interaction between the platform mass, flexures, mechanical linkages, and actuators. As a result, the fastest possible open-loop scan frequency is generally limited to less than 10% of the resonance frequency [16], [17] to avoid excitation of the mechanical resonance. Although control strategies can be developed to control the stage motion accurately at low speeds, these slow speeds of the XY stage lead to inordinate waiting periods which significantly affects the throughput of the manufacturing system. In addition to the low resonance frequency, these XY stages are often only lightly damped due to their lack of friction which makes them difficult to control. Owing to these reasons, unwanted exogenous disturbances (mechanical vibrations from other tools in on the shop floor, people walking near the tool, etc.) can excite the system and thus degrade the performance of the XY stage substantially [18].Consequently, the two main challenges in designing a controller for the stage are: 1) to track input signals with frequencies larger than the most dominant resonant frequency of the stage and 2) to reduce the resonance peak magnitude, i.e., to increase the damping so as to minimize the effects of exogenous disturbances on the stage. Many active damping controllers have been reported in literature for a range of applications including nanopositioning stages [19], [20], disk drives [21], [22] and high-speed AFM [23] among others. Some of the active damping control techniques such as Positive Position Feedback (PPF), Positive Velocity and Position Feedback (PVPF), Linear Quadratic Gaussian (LQG), Linear Quadratic Regulator (LQR) are computationally complex and difficult to implement while others such as Integral Force

Feedback (IFF) and Integral Resonant Control (IRC) are much easier to design and implement. Although a finite time horizon LQR controller is computationally expensive compared to IFF and IRC controls, it provides excellent stability robustness [24], good damping [25]–[27] and tracking [28] performance compared to classical controllers such as PID control [29] and full state feedback control using pole placement [25].

A short study comparing the performance of the finite horizon LQR and IRC-based controllers for the stage presented in this paper is included in the supplementary information (see supplementary information S1 for details on the study). Overall, the controller effort requirement for the IRC based controller is found to be significantly higher than that using a finite LQR controller. Thus, a finite time horizon LQR controller is designed and implemented on the XY stage for this study. The controller is also modified by appending a resonant shifting control action to the finite LQR to improve the positioning bandwidth of the stage.

## II. DESIGN OF XY NANOPOSITIONING STAGE

Flexure bearings have been widely used to achieve a long motion range with sub-micron resolution owing to their minimal friction, backlash, and hysteresis [30], [31]. Between the two broad categories of flexure-based stages (serial kinematic and parallel kinematic), a parallel kinematic design provides a better alternative for high speed, long range motion system with good accuracy. This can be attributed to the lower inertia of the its moving stage as compared to a serial kinematic stage design, its higher resonance frequency, and its higher mechanical stiffness along the actuation direction which leads to better positioning accuracy [32]. Many two-dimensional flexure based parallel-kinematic positioning stages have been proposed by researchers. The authors have also presented the design of a 50 mm travel flexure mechanism based on a DPF design [3], [15]. However, a DPF bearing enables both the intermediate stage and final stage to have same degrees-of-freedom and thus, leads to unwanted degrees-of-freedom (DoFs) on the intermediate stages which can lead to poor controller performance if the modes corresponding to resonance of intermediate stages fall in the operating frequency range. Thus, a modified DPF design (see supplementary Fig. S7) has been presented in [15] to eliminate the unnecessary degrees-of-freedom from the stage design and reduce the higher order resonant modes of the stage that cannot effectively be controlled.

This nested linkage design in the modified DPF eliminates the underconstraint commonly encountered when using a DPF based stage without increasing the overall footprint of the stage [33]. Detailed parametric design of the modified DPF bearing has been discussed in [33], [34] and static and dynamic performance of the 50 mm travel stage using modified DPF bearing have been identified by the authors in [15].

## III. EXPERIMENTAL SETUP AND SYSTEM IDENTIFICATION

The flexure stage is waterjet cut out from a 0.5" thick Al 7075 plate. Al 7075 is chosen due to its high yield stress limit. Two voice coil actuators are connected to the top and bottom levels of the assembly for actuation along X and Y axis independently. The experimental setup of the stage is shown in Fig. 1 and the assembly steps have been illustrated in [15]. For system identification and control design validation, the position output is measured using a capacitive sensor (model: C5-2.0, from Lion Precision- 1 nm resolution at 1 kHz within the measurement range of 250 μm [35]) due to its ease of setup and displacement data access. The μ-SLS employs an interferometer (model: FPS3010, from Attocube Systems AG) with a resolution of 1 pm and a working range of 2 m. The interferometer is also used to validate the 50 mm travel range of the stage (see supplementary Fig. S8). For actuation and sensor measurement, a National Instruments (NI) cRIO-9033 real-time controller equipped with NI-9263 analog output module and NI-9239 analog input module, is employed to produce excitation signals and acquire sensor readings, respectively. LabVIEW VIs have been developed for data collection and actuation for the nanopositioning system.
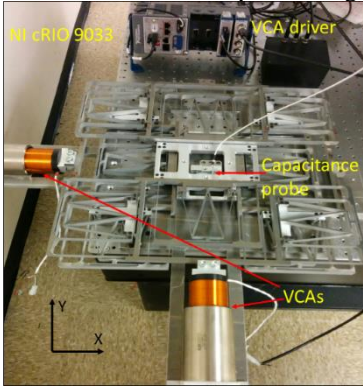


Fig. 1. Experimental setup for system identification of the stage[15]

The stiffnesses of the motion stage along x and y-axis are measured to be 1187 ± 166 N/m and 1157 ± 162 N/m respectively. The gains of the current amplifier, stiffness of the stage and other gains of interest have been depicted in the block diagram in Fig. 2. The block diagram depicts the flow of signals in open loop from the input signal (desired displacement) to actual displacement of the stage (output signal).The first block depicts the DC gain of the transfer function between input voltage and output displacement of the stage. The DC gain is estimated by measuring the static displacement of the stage for every input DC voltage and obtaining the slope of the fitted line between the input voltage and output displacement. Power amplifier's gain is set at 1 A/V and the force constant of the VCA (as provided by the manufacturer) is 14.6 N/A. The final block in the block diagram is the compliance of the XY stage for motion along y-axis.
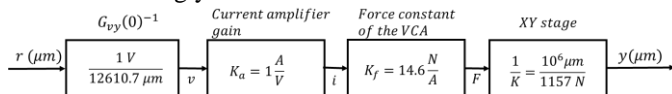


Fig. 2. DC gain values of different elements in the open loop experimental setup for y-axis motion

For system identification of the stage, a gaussian white noise signal with a standard deviation of 3.5 mV is used. This standard deviation of input voltage amplitude corresponds to a static standard displacement of 44 μm of the stage. The signal is sampled at 1000 Hz so as to capture the dynamics of the stage below 500 Hz. From the FEA simulations [15], the first few dominant modes of the stage are well within the 200 Hz frequency range and thus, a sampling rate of 1000 Hz is fast enough to capture the relevant dynamics of the stage. Input and output signals are chosen to be the desired displacement and the actual displacement of the stage respectively for estimating a linear model for the system. The maximum operating frequency of the stage for μ-SLS system is limited by the minimum sintering exposure duration. This frequency has an upper bound of 20 Hz, as the optimum sintering time for good sintering quality has been estimated experimentally to be 50 ms [36](see supplementary Fig. S9 for SEM image of a sintered spot). A transfer function estimate that accurately predicts the response of the system up to 2-3 times the maximum possible operating frequency is adequate for designing a closed loop control. From the experimental response of the stage (see Fig. 3), only the fundamental resonance peak falls within that frequency range (up to 60 Hz). Thus, a $2^{nd}$ order linear model estimate of the frequency response of the system is sufficient for closed loop control design up to desired operating frequencies. $2^{nd}$ order linear models are fitted to the frequency response of the plant along x and y axes and are given below.

$$G_{XX}(s) = \frac{778.6}{s^2 + 7.889\,s + 745.3} \quad (1)$$

$$G_{YY}(s) = \frac{712.2}{s^2 + 6.591s + 717.7}$$

Fig. 3 shows the magnitude plots of the experimentally obtained frequency response with the fitted transfer functions given by equation 1. The fitted transfer functions accurately predict the repsonse of the stage up to 60 Hz – 70 Hz.
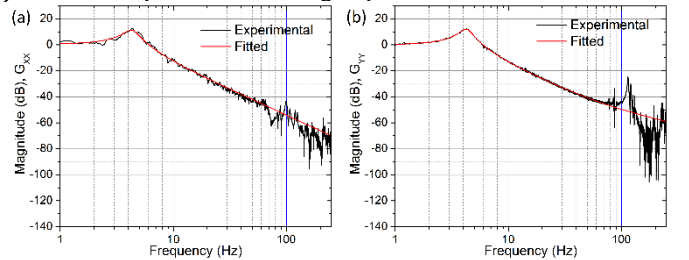


Fig. 3. Magnitude plots of fitted transfer function and experimental frequency response of the stage showing a good agreement between the two upto 70Hz (a) $G_{XX}$ (b) $G_{YY}$

To maximize the throughput of the sintering process, it is desired that the stage should be able to operate at frequencies ≈10 Hz i.e. the sintering time constitute the middle 50% of the step time duration. The 10 Hz required frequency is well above the 4.2 Hz natural frequency of the stage making it necessary to implement a closed loop control scheme on the stage in order to meet the throughput requirements of the μ-SLS system.

### A. Open loop response

The stage will need to traverse steps at a maximum frequency of 10 Hz (or some derivative of it- ramp-hold-ramp) in actual operation for laser sintering experiments and achieve sub-micron motion accuracy. The system is open loop stable as the poles of the system (-3.2955 ± 26.5864i) are located in the left half of σ = 0 on the s-plane. Fig. 4 shows the experimental open loop tracking performance of the stage along y-direction to steps of two different frequencies- 2 Hz and 10 Hz. For the slower steps at 2 Hz, though the stage tracks the reference trajectory, damping is extremely low which makes it impossible to achieve the desired accuracy within the time interval of the step. It is also interesting to note that the overshoots and undershoots for the steps are very large, with the overshoots going up to 66% higher than the desired step size. For 10 Hz signal, the stage is hardly tracking as the step times are smaller than the fundamental period of the stage motion and, thus, the stage is not even able to complete one full oscillation for each step. There is a need to design a closed loop controller to improve the tracking performance and damp the natural resonance of the stage. The next sections include the design of closed loop controller and the experimental verification of the controller.
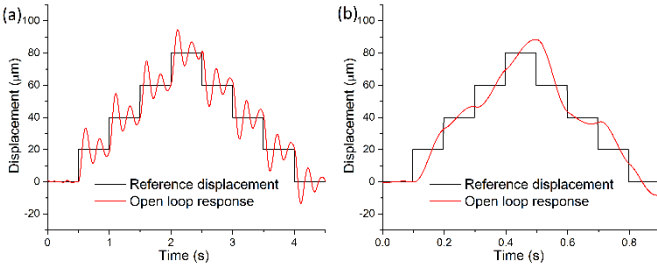


Fig. 4. Open loop tracking performance for a) 2 Hz steps b) 10 Hz steps

## IV. CLOSED LOOP CONTROL DESIGN

The control objective for the stage is to track reference signals with good accuracy and minimum control effort, achieve a bandwidth >10Hz and robustness to model uncertainties. Since the model of the XY stage is known beforehand with good confidence, a finite horizon LQR controller is suitable to achieve the desired performance owing to its robustness - for a single input-single output system, an LQR control achieves a phase margin of at least 60° and an infinite gain margin and is also robustly stable for small modeling errors [37]. Due to the decoupled static and dynamic behavior of the XY stage, independent control schemes can be designed for each axis[15]. This section illustrates the finite horizon LQR controller design for y-axis motion. Similar controller is also designed for x-axis motion. For designing an LQR controller, the transfer function model of the plant is converted to a state space model.

$$\dot{x} = Ax + Bu \tag{2}$$
$$y = Cx + Du$$

where,

$$A = \begin{bmatrix} -6.591 & -717.7 \\ 1 & 0 \end{bmatrix}; B = \begin{bmatrix} 1 \\ 0 \end{bmatrix}; C = [0 \quad 712.2]; D = 0$$

Before designing a feedback controller, it is important to verify that the controllability matrix is not rank deficient. From the canonical form of the state variables, it is evident that the system is both controllable and observable. In order to determine the optimal control inputs for tracking the reference variable at all times while optimizing the state variables, the following quadratic cost function is used where $P$ is the final time weighted matrix for the output, $Q$ is the transient time weighting for the output, and $R$ is the control input weighting:

$$V = \frac{1}{2}\big(Cx(T) - r(T)\big)^T P\big(Cx(T) - r(T)\big) \tag{3}$$
$$+ \frac{1}{2}\int_0^T \big((Cx(t) - r(t))^T Q\big(Cx(t) - r(t)\big) + u^T Ru\big)dt$$

Here, $Q$ is required to be at least positive semi-definite and $R$ is required to be a positive definite matrix. For obtaining the controller effort, it is assumed that all the states are available for feedback.

The controller effort to minimize the cost function is given by

$$u = -R^{-1}B^T(S(t)x(t) - v(t)) \tag{4}$$

where, $S(t)$ is the symmetric solution to the Ricatti differential equation

$$\dot{S} = -A^T S - SA + SBR^{-1}B^T S - C^T QC \tag{5}$$
$$with\ S(T) = C^T PC, \qquad S(t) = \begin{bmatrix} s_1(t) & s_2(t) \\ s_2(t) & s_3(t) \end{bmatrix}$$

Kalman gain sequence, $K$ is given by

$$K(t) = R^{-1}B^T S(t) \tag{6}$$

And $v(t)$ is the auxiliary function which can be found by solving the differential equation

$$\dot{v} = -(A - BK)^T v - C^T Qr \tag{7}$$
$$with\ v(T) = C^T P\,r(T)$$

These differential equations are solved using Euler's fixed step integration technique and are propagated backwards in time from the final time. When implementing the controller, the two state feedback signals are derived from a linear combination of position measurement and its derivative. Since the feedback gain matrix, K is varying in time, it can be calculated for all the time steps beforehand and stored in a look up table and then loaded when needed. The details of the finite LQR problem design and its variants can be found in literature [38], [39].

## V. EXPERIMENTAL RESULTS

### A. Step response

The performance of the controller is evaluated in terms of performance characteristics such as rise time, settling time, overshoot, and bandwidth obtained from the step response of the closed loop system. From the time response plot (see Fig. 5a), the closed loop response is much better compared to the open loop response of the stage. The rise time for closed loop response is reduced to 16.2 ms from 39.2 ms in open loop and the settling time (within 4% of steady state value) in closed loop is found to be only 32 ms compared to 1267 ms in open loop. Similarly, the overshoot in closed loop is also found to be much smaller at 2.5% of the steady state value. When compared against the open loop overshoot (at 68.5% of steady state value), this is approximately a 27x reduction. Additionally, the resonance of the stage appears to be well damped in closed loop leading to an increase in tracking bandwidth of the stage. The 3dB bandwidth of the stage in closed loop is found to be 13.7

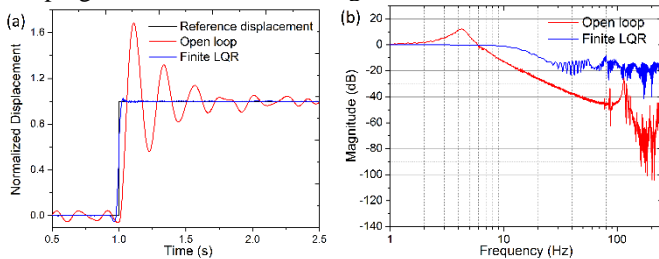Hz. This ascertains the effectiveness of the controller in damping the resonance of the stage.



Fig. 5. Open loop vs closed loop step response a) time-domain response b) magnitude plot of frequency response

### B. Resolution

The effect of resonance damping can also be corroborated by the difference in the positioning noise amplitudes of the system in open and closed loop (see Fig. 6). The $1\sigma$ noise level (see supplementary S2) in closed loop is found to be less than 8 nm which is about 8 times smaller than the noise in open loop.
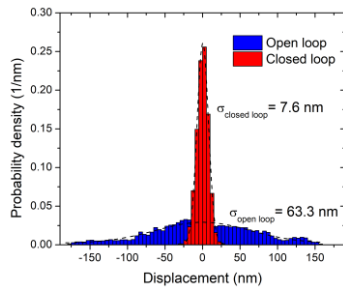


Fig. 6. Probability distribution of open and closed loop positioning noise amplitudes

### C. Tracking performance

To illustrate the time domain tracking performance of the controller designed, steps of different magnitudes ranging from 40 nm to 20 µm are fed at different frequencies (2 Hz, 4 Hz and 10 Hz) as the reference input to the closed loop system. It can be clearly observed that the controller works very well when tracking 2 Hz signals (Fig. 4, 7a and 8a show the comparison of open and closed loop performance) and the root mean squared error (RMSE) for tracking is found to be still within 8 nm for 1 µm steps and less than 44 nm for 20 µm steps. Although the tracking errors are not as small at 10 Hz as at 2 Hz, the stage is still able to track the reference with good accuracy (see Table 2) for the sintering duration requirement and is found to be a significant improvement over the open loop tracking at 10 Hz (see Fig. 4b and 8a for comparison). The RMS errors for these step tracking signals are calculated as the average of the RMS errors calculated over each step in the middle 50% of the step duration (See supplementary information S3 for details on the calculation). Table 2 lists the RMS positioning error in tracking signals of different amplitudes at different tracking speeds.

Table 2. RMS positioning error (in nm) while tracking steps of different frequencies and different amplitudes for middle 50% of the step duration

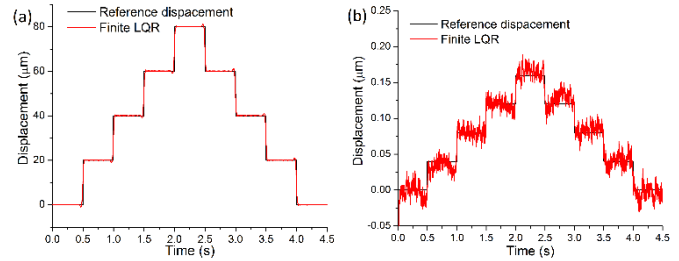| Tracking speed | Step amplitude | | |
|---|---|---|---|
| | 1 µm | 10 µm | 20 µm |
| 2 Hz | 8 ± 1 | 18 ± 1 | 44 ± 6 |
| 4 Hz | 10 ± 4 | 34 ± 10 | 44 ± 4 |
| 10 Hz | 31 ± 14 | 254 ± 94 | 576 ± 161 |



Fig. 7. Closed loop tracking performance along y-axis for a) 20 µm b) 40 nm steps with a step frequency of 2Hz
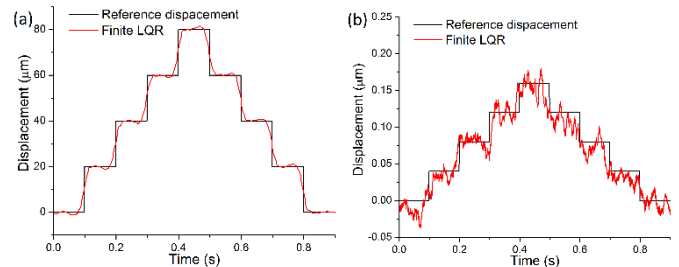


Fig. 8. Closed loop tracking performance along y-axis for a) 20 µm b) 40 nm steps with a step frequency of 10Hz

In addition to the step signals, the controller is also tested for triangular trajectory tracking and the tracking errors in closed loop are reduced significantly at all signal frequencies (see Table 3 and supplementary information S4).

Table 3. RMS errors for triangular tracking in both open loop and closed loop

| Tracking speed | Open loop (nm) | Closed loop (nm) |
|---|---|---|
| 2 Hz | 1281 ± 146 | 130 ± 15 |
| 4 Hz | 8012 ± 283 | 197 ± 19 |
| 10 Hz | 3629 ± 174 | 522 ± 36 |

Similar tracking performance tests were also conducted with x-axis motion of the stage to verify the resolution and performance. Since the static and dynamic performance of the stage along both axes are nearly identical, the results obtained were similar.

### D. 2D tracking

For evaluating the 2D motion tracking performance of the stage, a circle of 100 µm diameter is tracked at different speeds- 0.1 Hz, 0.5 Hz, 2 Hz, 4 Hz and 10 Hz. This is achieved by sending sinusoidal inputs separated by a phase of 90° to the x and y axes of the stage. Fig. 9 shows the reference trajectory and the actual path covered when the stage is tracking the circle at 0.5 Hz. The radial errors have been amplified by 10 and 50 times for better visualization. The $1\sigma$ radial error for tracking a 100 µm diameter circle at 0.5 Hz is found to be 125 nm as against 1869 nm in open loop. Table 4 compares the open loop 2D tracking parameters- mean radius and $1\sigma$ radial error, with the closed loop 2D tracking parameters for 100 µm diameter circle tracking at different speeds.

Table 4. Mean radius and $1\sigma$ radial errors for 100 µm diameter circle tracking at different speeds

| Tracking speed (Hz) | Open loop mean radius (µm) | Open loop $1\sigma$ radial error (nm) | Closed loop mean radius (µm) | Closed loop $1\sigma$ radial error (nm) |
|---|---|---|---|---|
| 0.5 | 48.98 ± 0.02 | 1869 ± 9 | 49.92 ± 0.00 | 125 ± 5 |
| 2 | 54.55 ± 0.09 | 2024 ± 96 | 49.64 ± 0.04 | 194 ± 28 |

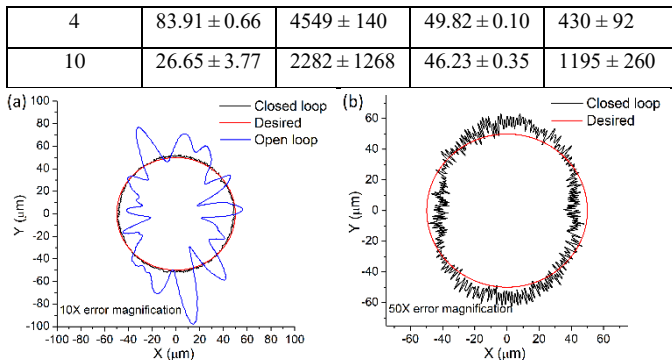| 4 | 83.91 ± 0.66 | 4549 ± 140 | 49.82 ± 0.10 | 430 ± 92 |
| 10 | 26.65 ± 3.77 | 2282 ± 1268 | 46.23 ± 0.35 | 1195 ± 260 |



Fig. 9. XY stage tracking a 100 μm circle at 0.5 Hz in a) open and closed loop with radial errors magnified 10x for better visualization b) closed loop with radial errors magnified 50x

## VI. MODIFIED CONTROL DESIGN

The tracking bandwidth of the closed loop system can further be increased by using a resonant shifting controller in addition to the finite horizon LQR control. Using the algorithm described in [40], a proportional gain is included in the negative feedback loop (see supplementary Fig. S2.a) to shift the resonance of the stage and the effect of changing the shifting gains is illustrated by the frequency response magnitude plot of the closed loop in Fig. 10.
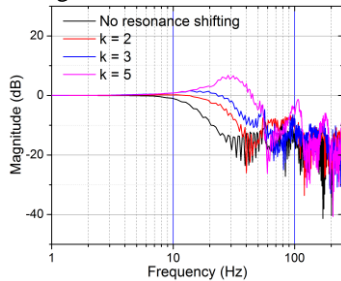


Fig. 10. Experimentally measured frequency response (magnitude plot) of the closed loop with different resonant shifting gains

Without any resonance shifting control, the closed loop response is almost flat at 0 dB magnitude up to 8 Hz and the resonance of the stage has been damped effectively leading to a 3 dB bandwidth of 13.7 Hz. Though the 3dB bandwidth of the closed loop response increases as the resonance shifting gain, k is increased, the frequency response magnitude displays an increasing upward deviation from 0 dB value leading to large overshoots in tracking and thus, longer settling times. This is due to the fact that although the resonant shifting control shifts the resonance frequency by a factor (see supplementary information S.1.1), it also lowers the damping coefficient by the same factor leading to higher resonant peaks. Through trial and error, the resonant shifting gain that improved the bandwidth without magnifying the gain amplitude is found to be when the shifting gain is 2. With k = 2, the 3 dB bandwidth of the closed loop response is found to be 23 Hz. Fig. 11 shows the tracking performance comparison of the finite LQR controller with finite LQR+ resonant shifting controller at three different operating frequencies- 10 Hz, 15 Hz and 20 Hz. At all three speeds, it is evident that the tracking performance of the finite LQR+ resonant shifting controller is better than just the finite LQR

controller. This is also corroborated by the RMS tracking errors presented in Table 5 for the two cases. The average RMS errors are reduced by 12%, 31% and 48% for 10 Hz, 15 Hz and 20 Hz stepping speeds by using the resonant shifting control with Finite LQR (RMS errors are calculated the same way as described in Section V C) and thus providing better accuracy compared to the Finite LQR only controller.
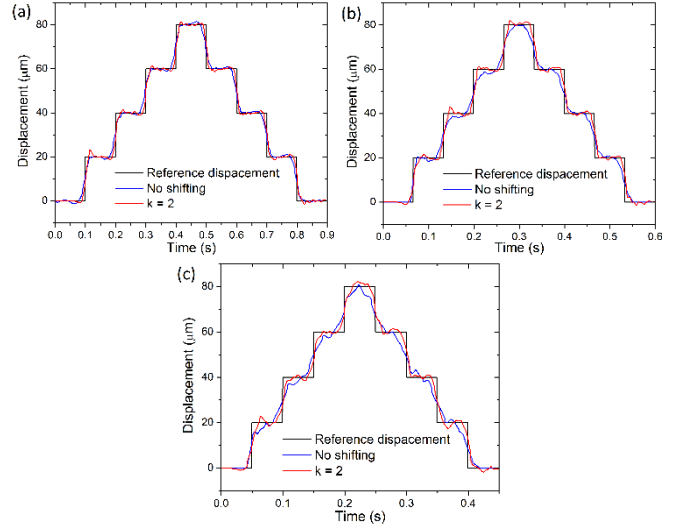


Fig. 11. Closed loop tracking performance comparison between 'Finite LQR only' and 'Finite LQR+ Resonant shifting' control for motion along y-axis with a step frequency of a) 10 Hz b) 15 Hz and c) 20 Hz

Table 5. RMS tracking error (in nm) comparison between a controller with both Finite LQR and resonant shifting and a controller with only Finite LQR, while tracking 20 μm steps of different frequencies

| Tracking speed | RMS error of step tracking performance (nm) | |
| --- | --- | --- |
| | Without resonance shifting control | With resonance shifting control |
| 10 Hz | 534 ± 120 | 469 ± 118 |
| 15 Hz | 1006 ± 366 | 695 ± 150 |
| 20 Hz | 1949 ± 259 | 1021 ± 406 |

## VII. IMPLEMENTATION SCHEME FOR FULL TRAVEL RANGE

The controller design is shown to work effectively in tracking when the stage behavior is linear with constant stiffness and minor variations in stiffness are taken care of by the robustness of the controller. However, at large displacements of the stage, the stage behavior changes and stiffness increases. To account for this changing behavior, the controller design will be replicated to different domains of the stage motion. The whole travel range ($x_0=0$ to $x_n= 50$ mm) will be broken down into n small travel ranges ($x_0$-$x_1$, $x_1$-$x_2$…… $x_{n-1}$ to $x_n$) such that the stiffness over each travel range is almost constant with minor variations i.e. the stage can be modeled as a linear system in each of these n ranges. The controller design will be updated with different stiffnesses for each of those small travel ranges. Based on the position of the stage, the corresponding controller will be implemented to achieve the desired step size. The stage will traverse a maximum step size of 2 mm during which the stiffness of the stage can be approximated as a constant and

hence, the control action can be extended to cover the entire travel range. Additionally, using a parallel kinematic design makes it possible to accurately characterize the parasitic motion which can be easily calibrated during closed loop operation of the stage over the full travel range.

## VIII. DISCUSSION AND CONCLUSION

Table 6. Performance characteristics of the XY stage

| Performance parameters | Value |
|---|---|
| Open loop resolution | 63 nm |
| Closed loop resolution | 8 nm |
| Minimum step size* (with an SNR = 2 at 10 Hz) | 14 nm |
| Max. operating speed# in Open loop (3dB) | 2.4 Hz |
| Max. operating speed with Finite LQR only | 13.7 Hz |
| Max. operating speed with Finite LQR and resonant shifting control | 23.0 Hz |
| Motion range | 50 mm X 50 mm |
| Dynamic range | 136 dB |

* 'Minimum step size with an SNR of 2' is defined as twice the minimum standard deviation (calculated for the middle 50% of the step duration) of the tracking signal while tracking steps of different amplitudes (20 nm to 20 μm) at a speed of 10 Hz (see supplementary information S5)

# 'Max. operating speed' is the frequency at which the frequency response plot (magnitude) first crosses ±3 dB indicating a magnification (corresponding to 3dB)/attenuation (corresponding to -3dB) in amplitude of the tracked displacement signal compared to the desired reference signal, both of which are equally bad for reference tracking (see Figures 5b and 10)

This paper illustrates the need for an XY nanopositioner in the μ-SLS system briefly. As per the requirements of the μ-SLS process, the stage is required to have a travel range of 50 mm along each working axes of the stage with sub-micron resolution and 10 Hz tracking bandwidth. The key performance parameters of the XY nanopositioning stage have been summarized in Table 6. The 2D stage can achieve a long 50 mm stroke in either axis. Since the motion is decoupled and design is identical along both axes, the performance parameters are similar for both motion axes. The open loop resolution of the stage is found to be 63 nm. This noise estimate is a combination of the mechanical noise, sensor noise and actuator noise with mechanical noise being the major contributor due to the low resonance and poor damping of the stage in open loop.

The paper presents the design of an optimal LQR controller (finite horizon) based on the model derived from system identification of the stage. The controller is shown to effectively damp the resonance and the closed loop resolution is found to be 8 times smaller than open loop resolution at 8 nm. In addition, the tracking bandwidth which is typically limited to 10% of the resonance frequency for XY flexure stages has also been significantly improved and signals as fast as 10 Hz (2.5 X natural frequency) have been tracked successfully. To further enhance the bandwidth of the stage, a resonant shifting control is appended to the finite LQR controller and the combination of the two control actions is shown to work better than using only finite LQR control. The minimum step size in closed loop with a signal to noise ratio of 2 is found to be 14 nm at a tracking frequency of 10 Hz. Using the motion range of 50 mm and

resolution of 8 nm, the dynamic range of the stage is calculated to be 136 dB which is a significant improvement over the off the shelf stages or other stages developed in research labs. Fig. 12 depicts the range vs. resolution comparison of XY stage developed in this study with various stages presented in Table 1. This increased dynamic range and bandwidth will enable this type of flexure-based stage to be used in a variety of high-speed, large-travel applications including scanning nanometrology processes such as in-line inspection and process control in semiconductor industries and nanomanufacturing applications such as lithography and μ-SLS.
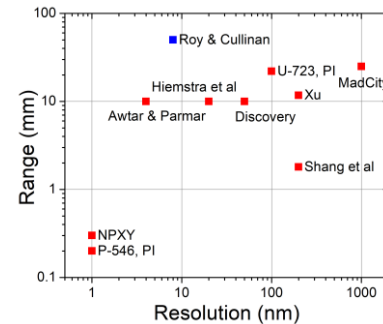


Fig. 12. Range vs resolution plot comparing the stage developed in this study with commercial stages and stages developed in other research labs; showing the larger range with finer resolution of the stage compared to others

## REFERENCES

[1] N. Roy, A. Yuksel, and M. Cullinan, "Design and modeling of a microscale selective laser sintering system," in *ASME 2016 11th International Manufacturing Science and Engineering Conference, MSEC 2016*, 2016, vol. 3, p. V003T08A002--V003T08A002.

[2] N. K. Roy, C. S. Foong, and M. A. Cullinan, "Design of a Micro-scale Selective Laser Sintering System," in *2016 Annual International Solid Freeform Fabrication Symposium*, 2016, pp. 1495–1508.

[3] N. Roy and M. Cullinan, "Design of a Flexure Based XY Precision Nanopositioner with a Two Inch Travel Range for Micro-Scale Selective Laser Sintering," in *Proceedings of the Annual Meeting of the American Society for Precision Engineering 31st Annual Meeting*, American Society for Precision Engineering, ASPE, 2016, pp. 395–400.

[4] Physik Instrumente, "PInano® Piezo Microscope Stage & Controller." [Online]. Available: PInano®%0APiezo Microscope Stage & Controller. [Accessed: 14-Oct-2017].

[5] npoint, "NPXY300-291 Nanopositioning Piezo Stage." [Online]. Available: https://www.npoint.com/products/nanopositioning-stages/item/npxy300-291/. [Accessed: 14-Oct-2017].

[6] Physik Instrumente, "U-723 PILine® XY Stage." [Online]. Available: https://www.physikinstrumente.com/en/products/xy-stages/stages-with-piezomotor/u-723-piline-xy-stage-1000583/. [Accessed: 14-Oct-2017].

[7] Mad City labs, "Nano-View/M Series." [Online]. Available: http://www.madcitylabs.com/nanoviewm.html. [Accessed: 14-Oct-2017].

[8] D. B. Hiemstra, G. Parmar, and S. Awtar, "Performance tradeoffs posed by moving magnet actuators in flexure-based nanopositioning," *IEEE/ASME Trans. Mechatronics*, vol. 19, no. 1, pp. 201–212, 2014.

[9] S. Awtar and G. Parmar, "Design of a large range XY nanopositioning system," *J. Mech. Robot.*, vol. 5, no. 2, p. 21008, 2013.

[10] Q. Xu, "Design and development of a compact flexure-based XY precision positioning system with centimeter range," *IEEE Trans. Ind. Electron.*, vol. 61, no. 2, pp. 893–903, 2014.

[11] J. Shang, Y. Tian, Z. Li, F. Wang, and K. Cai, "A novel voice coil motor-driven compliant micropositioning stage based on flexure mechanism," *Rev. Sci. Instrum.*, vol. 86, no. 9, p. 95001, 2015.

[12] Y. Choi, S. V Sreenivasan, and B. J. Choi, "Mechanism and Machine Theory Kinematic design of large displacement precision XY positioning stage by using cross strip flexure joints and over-constrained mechanism," vol. 43, pp. 724–737, 2008.

[13] L. L. Howell, *Compliant mechanisms*. John Wiley & Sons, 2001.

[14] G. Hao and X. Kong, "A novel large-range XY compliant parallel manipulator with enhanced out-of-plane stiffness," *J. Mech. Des.*, vol. 134, no. 6, p. 61009, 2012.

[15] N. K. Roy and M. A. Cullinan, "Design and characterization of a two-axis, flexure-based nanopositioning stage with 50 mm travel and reduced higher order modes," *Precis. Eng.*, 2018.

[16] Y. R. Teo, D. Russell, S. S. Aphale, and A. J. Fleming, "Optimal integral force feedback and structured PI tracking control: Application for objective lens positioner," *Mechatronics*, vol. 24, no. 6, pp. 701–711, 2014.

[17] S. O. R. Moheimani, "Invited review article: Accurate and fast nanopositioning with piezoelectric tube scanners: Emerging trends and future challenges," *Rev. Sci. Instrum.*, vol. 79, no. 7, p. 71101, 2008.

[18] I. R. Walker, *Reliability in scientific research: improving the dependability of measurements, calculations, equipment, and software*. Cambridge University Press, 2011.

[19] S. Verma, W. Kim, and J. Gu, "Six-axis nanopositioning device with precision magnetic levitation technology," *IEEE/ASME Trans. Mechatronics*, vol. 9, no. 2, pp. 384–391, 2004.

[20] J. L. Fanson and T. K. Caughey, "Positive position feedback control for large space structures," *AIAA J.*, vol. 28, no. 4, pp. 717–724, 1990.

[21] H. Numasato and M. Tomizuka, "Settling control and performance of a dual-actuator system for hard disk drives," *IEEE/ASME Trans. mechatronics*, vol. 8, no. 4, pp. 431–438, 2003.

[22] M. A. Hawwa and J. Bozorgi, "Piezoelectric vibration damping for disk drives." Google Patents, 2001.

[23] N. Kodera, H. Yamashita, and T. Ando, "Active damping of the scanner for high-speed atomic force microscopy," *Rev. Sci. Instrum.*, vol. 76, no. 5, p. 53708, 2005.

[24] B. D. O. Anderson and J. B. Moore, *Linear optimal control*, vol. 197, no. 1. Prentice-Hall Englewood Cliffs, NJ, 1971.

[25] E. V. Kumar and J. Jerome, "Robust LQR controller design for stabilizing and trajectory tracking of inverted pendulum," *Procedia Eng.*, vol. 64, pp. 169–178, 2013.

[26] W. Jarzyna, M. Augustyniak Michałand Bochenski, and J. Warminski, "PD and LQR controllers applied to vibration damping of an active composite beam," *Prz. Elektrotechniczny*, vol. 88, no. 10B, pp. 128–131, 2012.

[27] W. Jarzyna, M. Augustyniak, J. Warmiński, and M. Bocheński, "State control with LQR algorithms applied in vibration damping of cantilever beam," in *Power Electronics and Motion Control Conference (EPE/PEMC), 2012 15th International*, 2012, p. DS1c-.8.

[28] R. A. Braker and L. Y. Pao, "Fast setpoint tracking of an Atomic Force Microscope X- Y stage via optimal trajectory tracking," in *American Control Conference (ACC), 2017*, 2017, pp. 2875–2881.

[29] A. N. K. Nasir, M. A. Ahmad, and M. F. Rahmat, "Performance comparison between LQR and PID controllers for an inverted pendulum system," in *AIP Conference Proceedings*, 2008, vol. 1052, no. 1, pp. 124–128.

[30] A. H. Slocum, *Precision machine design*. Society of Manufacturing Engineers, 1992.

[31] S. T. Smith, *Flexures: elements of elastic mechanisms*. CRC Press, 2000.

[32] A. J. Fleming and K. K. Leang, *Design, modeling and control of nanopositioning systems*. Springer, 2014.

[33] R. M. Panas and J. B. Hopkins, "Eliminating Underconstraint in Double Parallelogram Flexure Mechanisms," *J. Mech. Des.*, vol. 137, no. 9, p. 92301, 2015.

[34] R. M. Panas, "Large displacement behavior of double parallelogram flexure mechanisms with underconstraint eliminators," *Precis. Eng.*, vol. 46, pp. 399–408, 2016.

[35] IBS Precision Engineering, "Data sheet - LION Precision capacitive sensors."[Online].Available:http://www.ibspe.com/public/uploads/content/files/capacitive-data-sheet-EN.pdf. [Accessed: 05-Sep-2017].

[36] N. K. Roy *et al.*, "A Comprehensive Study of the Sintering of Copper Nanoparticles Using Femtosecond, Nanosecond, and Continuous Wave Lasers," *J. Micro Nano-Manufacturing*, vol. 6, no. 1, p. 10903, 2017.

[37] J.-B. He, Q.-G. Wang, and T.-H. Lee, "PI/PID controller tuning via LQR approach," *Chem. Eng. Sci.*, vol. 55, no. 13, pp. 2429–2439, 2000.

[38] F. L. Lewis, D. Vrabie, and V. L. Syrmos, *Optimal control*. John Wiley & Sons, 2012.

[39] K. Zhou, J. C. Doyle, K. Glover, and others, *Robust and optimal control*, vol. 40. Prentice hall New Jersey, 1996.

[40] M. Namavar, S. Member, A. J. Fleming, and S. S. Aphale, "Resonance-shifting Integral Resonant Control Scheme for Increasing the Positioning Bandwidth of Nanopositioners," pp. 1317–1322, 2013.

Michael A Cullinan received the B.S. degree in engineering and the B.A. degree in economics from Swarthmore College, Swarthmore, PA, USA in 2006. He received his M.S. and Ph.D. degrees in mechanical engineering from Massachusetts Institute of Technology, Cambridge, MA, USA in 2008 and 2011, respectively.

He is currently an Assistant Professor and the director of the Nanoscale Design and Manufacturing Lab (NDML) at UT Austin. Prior to joining the University of Texas, he was a National Research Council Postdoctoral Associate at the National Institute of Standards and Technology in Gaithersburg, Maryland. His research interests include the design and development of nanomanufacturing processes and equipment, the application of nanoscale science in engineering, the engineering of thin films, nanotubes and nanowires, the manufacturing and assembly of nanostructured materials, and the design of micro/nanoscale machine elements for mechanical sensors and energy systems.

Nilabh K Roy received the B.Tech degree in mechanical engineering from Indian Institute of Technology Delhi, India, in 2014. He is currently pursuing the Ph.D. degree in mechanical engineering from The University of Texas at Austin.

His research interests include design and development of microscale AM systems, laser-metal nanoparticle interactions, precision optics, precision flexure XY stage design, system identification, robust real time control design and roll to roll web modeling and control design.

List of Figures

Fig. 8. Closed loop tracking performance along y-axis for a) 20 µm b) 40 nm steps with a step frequency of 10Hz

Fig. 9. XY stage tracking a 100 µm circle at 0.5 Hz in a) open and closed loop with radial errors magnified 10x for better visualization b) closed loop with radial errors magnified 50x

Fig. 10. Experimentally measured frequency response (magnitude plot) of the closed loop with different resonant shifting gains

Fig. 11. Closed loop tracking performance comparison between 'Finite LQR only' and 'Finite LQR+ Resonant shifting' control for motion along y-axis with a step frequency of a) 10 Hz b) 15 Hz and c) 20 Hz

Fig. 12. Range vs resolution plot comparing the stage developed in this study with commercial stages and stages developed in other research labs; showing the larger range with finer resolution of the stage compared to others

## List of tables

Table 1. Range and resolution of various stages available commercially and developed in research labs

Table 2. RMS positioning error (in nm) while tracking steps of different frequencies and different amplitudes for middle 50% of the step duration

Table 3. RMS errors for triangular tracking in both open loop and closed loop

Table 4. Mean radius and 1σ radial errors for 100 µm diameter circle tracking at different speeds

Table 5. RMS tracking error (in nm) comparison between a controller with both Finite LQR and resonant shifting and a controller with only Finite LQR, while tracking 20 µm steps of different frequencies

Table 6. Performance characteristics of the XY stage